Composition-Tunable Optical Properties of Colloidal IV−VI Quantum Dots, Composed of Core/Shell Heterostructures with Alloy Components

Georgy I. Maikov, Roman Vaxenburg, Aldona Sashchiuk, and Efrat Lifshitz*

Schulich Faculty of Chemistry, Russell Berrie Nanotechnology Institute, Solid State Institute, Technion, Haifa 32000, Israel

ABSTRACT Colloidal quantum dots (CQDs) attract worldwide scientific and technological attention due to the ability to engineer their optical properties by the variation of their size. However, several important applications, such as biological tagging and photovoltaic cells, impose a limit on their size yet demand tunability and thermal stability of the optical band edge. This work introduces a new class of heterostructures, composed of PbSe or $PbSe_yS_{1-y}$ cores, coated by PbS or $PbSe_xS_{1-x}$ shells, with different core-radius/shell-width division, with a radial gradient composition (with $0 < y < 1$, $0 < x < 1$), which offer a control of the band edge properties by varying the CQDs' composition. Continuous-wave and transient photoluminescence measurements over a wide temperature range (1.4−300 K) revealed a distinct behavior of the heterostructures with respect to that of pure PbSe cores: (i) increase of the emission quantum yield; (ii) red-shift of the absorption edge but a decrease of the emission Stokes shift; (iii) alleviation of a dark exciton recombination, *viz.*, a reduction of an exchange interaction; (iv) tuning of the radiative lifetime with shell width and composition; (v) reduction of the band edge temperature coefficient, dE/dT, *viz.*, induction of thermal stability. The k · p envelope function calculation, considering abrupt or smooth alloying continuation of the potential at the core−shell interface, revealed a delocalization of the hole wave function over the entire volume of the CQDs, as a partial explanation for the marked tunability, nonetheless preserving a desired size.

KEYWORDS: lead chalcogenide · PbSe · core/shell · alloyed quantum dots · core/alloyed-shell · composition-tunable optical properties

Colloidal semiconductor nanocrystals attract worldwide scientific and technological interest due the ability to engineer their optical properties by the variation of size, shape, and surface properties.[1−3] Recent studies revealed new strategies related to composition control of the properties, including alloying,[4−7] doping,[8] and in particular the formation of core/shell heterostructures.[9−14] The concept of heterostructuring has been known for years in the field of epitaxial quantum wells and superlattices, rendering direct manipulation of electronic structure by varying the structural subunit's width and composition.[15] This concept was adapted to the field of colloidal quantum dots (CQDs) more than a decade ago.[9−14] A typical approach at that time utilized a wide-gap semiconductor that epitaxially covered a narrow-gap semiconductor to form the so-called core/shell structure, which chemically passivates surface-related trapping sites. Moreover, the existence of a wide-gap semiconductor shell enables electronic wrapping of the core's band edges by those of the exterior shells, which further confines the electron and hole into the core regime (type-I electronic alignment), leading to a substantial improvement in the emission quantum yield (QY). Advances in the colloidal chemistry procedures led to a later development of type-II core/shell quantum dots[11−13] and quantum rods,[15,16] in which the electronic alignment throughout the core/shell structure causes spatial separation of the electrons and holes between the two regimes, or the formation of a *quasi*-type-II behavior in which only one of the carriers is delocalized over the entire core/shell structure.[11,12] Type-II and *quasi*-type-II heterostructures provide interesting opportunities for tuning the electronic band gap,[17] luminescence lifetime,[18] and carrier−carrier interactions.[19]

Whereas major effort has been devoted to the development of II−VI core/shell structures,[12−17] there are only a few reports concerning the heterostructures of IV−VI CQDs. The pioneering work of Sashchiuk *et al.*[20] and Brumer *et al.*[21] showed the synthesis of PbSe/PbS core/shell CQDs revealing a chemical stability of the heterostructures over months at ambient conditions, with a shell width >2 monolayers (with monolayer width of 0.6 nm) when stored in a powder form and photostability under visible and/or near-infrared excitation (avoiding a UV pumping under oxygen environment).[22,23] This innovative work was followed by a

*Address corespondence to ssefrat@technion.ac.il.

Received for review July 25, 2010 and accepted October 04, 2010.

Published online October 14, 2010. 10.1021/nn101760t

few successful efforts in the formation of PbSe/PbS CQDs at a low temperature and pressure and growth of a PbS shell by successive ion layer adsorption and reaction (SILAR) method.[24] Recent studies showed the synthesis of PbSe/CdSe and PbSe/CdSe/ZnSe core/shell heterostructures, using an ion exchange chemical procedure for the shell formation.[25] The IV−VI heterostructures mentioned, with band edge tunability in the near-infrared, could be used in gain devices,[26,27] photovoltaic cells,[28−34] spintronics,[35,36] and biological labeling.[37−39]

Band gap tunability can also be gained in homogeneous alloyed materials, such as $CuIn_xGa_{1-x}Se_2$,[40] $CdE'_yE''_{1-y}$ (E′ and E″ are two different chalcogenes),[41,42] $Cd_xHg_{1-x}Te$,[43] $Cd_xZn_{1-x}S(Se)$,[44] and $PbSe_xS_{1-x}$,[5] all obeying Vegard's law change in the crystallographic parameters and corresponding tuning of the band gap. However, these nanocrystals do not offer tunability of carrier localization, often crucial in technological devices. Thus, currently the most sophisticated structures involve the integration of a core/shell heterostructure with a potential interface, combined with an alloy composition of either the core or the shell (or both), such as $PbSe/PbSe_xS_{1-x}$,[14] $Cd_xZn_{1-x}Se/ZnSe(S)$,[45] $CuInS_2/ZnS$,[46] and $CdTe/CdTe_xSe_{1-x}$,[47,48] allowing a gradient composition (when $0 < x < 1$) from the center to the exterior surface. For example, $PbSe/PbSe_xS_{1-x}$ and $CdTe/CdTe_xSe_{1-x}$ core/alloyed-shell CQDs showed an emission QY up to ~90% and exceptional chemical stability.[21,23,45,47] Recent studies[47,49] involving the investigation of $CdTe/CdTe_xSe_{1-x}$ and $Cd_xZn_{1-x}Se/ZnSe(S)$, having a *quasi*-type-II configuration, offered the ability to suppress interrupting Auger relaxation, thus stabilizing emission intensity (blinking free behavior) and extending the lifetime of multiple excitons to a nanosecond regime, phenomena with valuable benefits in using the CQDs in gain devices[26,27] and photovoltaic cells.[28−34]

On the basis of the information given, a combined strategy between core/shell heterostructuring and alloying should offer tunability of the core/shell interface's strain,[18,50] band edge offset or/and warping,[10−12] and delocalization of carriers.[51] While several reports express the merits of this combination in II−VI CQDs,[1,11,12,17] there is little work on IV−VI based CQDs. Considering the significant potential of the IV−VI heterostructures in several of the applications mentioned, the present work describes the structural and optical characterization of PbSe/PbS core/shell (c/sh), $PbSe/PbSe_xS_{1-x}$ core/alloyed-shell (c/a-sh), and newly prepared $PbSe_yS_{y-1}/PbSe_xS_{1-x}$ alloyed-core/alloyed-shell (a-c/a-sh) CQDs, with variable internal diameters and a radial gradient composition (when $0 < x < 1$, $0 < y < 1$). A thorough investigation of the optical properties was performed by following the variable temperature continuous-wave (cw) and transient photoluminescence (PL) spectra, exploring energy shift, band edge temperature coefficient, alleviation of a dark−bright splitting (or exchange interaction),

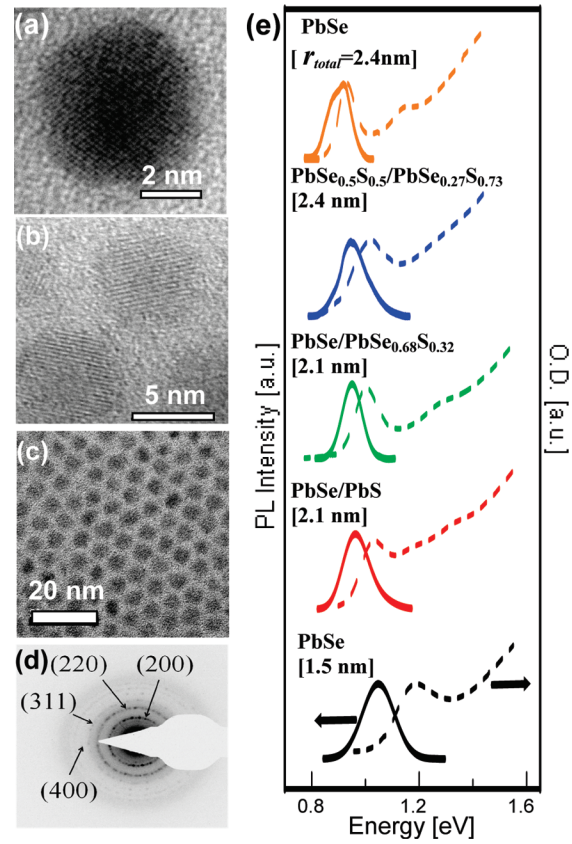

Figure 1. Representative HR-TEM image of (a) single $PbSe_{0.5}S_{0.5}/PbSe_{0.27}S_{0.73}$ alloyed-core/alloyed-shell CQD with an overall radius (r_{total}) of 2.0 nm and (b) PbSe/PbSe core/shell CQD with a core radius (r_{core}) of 2.5 nm and overall radius of 5 nm. (c) TEM image of an ensemble of CQDs shown in panel a. (d) SAED image of the CQDs in panel c. (e) Absorption (dashed lines) and emission (solid lines) spectra of PbSe core (bottom and top curves), PbSe/PbS core/shell, PbSe/$PbSe_{0.68}S_{0.32}$ core/alloyed-shell, and $PbSe_{0.5}S_{0.5}/PbSe_{0.27}S_{0.73}$ alloyed-core/alloyed-shell CQDs with overall radius, r_{total}, as labeled in panel e and measured at room temperature. The core radii of the heterostructures presented in panel e are in accordance with Table 1.

valley−valley interaction, emission quantum yield, and radiative lifetime of the heterostructures, in comparison with the existing properties of the primary PbSe core CQDs.[52] The results reflect the uniqueness of the electronic properties of the heterostructures, controlled by shell width and alloyed composition.

RESULTS AND DISCUSSION

The investigated CQDs were prepared by colloidal chemistry, according to the short description given below in Methods and a detailed procedure reported in ref 21. The structure and composition of the CQDs were characterized by the use of high-resolution transmission electron microscopy (HR-TEM), selected area electron diffraction (SAED), energy-dispersive analysis of X-ray (EDAX), inductively coupled plasma atomic emission spectroscopy (ICP-AES,) and X-ray photoelectron spectroscopy (XPS). Figure 1 represents HR-TEM images of $PbSe_{0.5}S_{0.5}/PbSe_{0.27}S_{0.73}$ (a) and PbSe/PbS (b) CQDs. These images reveal distinguished crystal planes, sup-

TABLE 1. Relevant Parameters[a] of the Investigated CQDs

molecular formula of CQDs	Pb [%]	Se [%]	S [%]	r_{core} [nm]	r_{total} [nm]	E_g exp. [eV]	E_g calc. [eV]	QY [%]	τ_{rad} [μs]	E_s [meV]
PbSe	51.5	48.5	0.0	1.5	1.5	1.17		48	2.99	112
PbSe	54.0	46.0	0.0	2.4	2.4	0.93	1.16	83	1.23	34
PbSe/PbS	55.2	17.1	27.7	1.5	2.1	1.03	1.10	65	2.62	55
PbSe/PbS	53.8	13.5	32.7	1.5	2.3	0.98	0.95	88	1.72	53
PbSe/$PbSe_{0.68}S_{0.32}$	50.0	40.0	10.0	1.5	2.1	1.00	1.14	68	2.21	75
$PbSe_{0.5}S_{0.5}$	50.8	25.1	24.2	1.6	1.6	1.18		27	5.50	103
$PbSe_{0.5}S_{0.5}$/$PbSe_{0.24}S_{0.76}$	49.2	20.3	30.5	1.6	1.9	1.09	1.40	46	2.37	73
$PbSe_{0.5}S_{0.5}$/$PbSe_{0.27}S_{0.73}$	48.8	17.5	33.7	1.6	2.4	1.02	0.97	65	1.96	45

[a]band gap energy (E_g), quantum yield (QY), radiative lifetime (τ_{rad}) and Stokes shift (E_s), all at room temperature.

porting high crystallinity of the a-c/a-sh CQDs. In most cases the core−shell interface is indistinguishable in $PbSe_{0.5}S_{0.5}$/$PbSe_{0.27}S_{0.73}$ CQD (panel a) because of the close proximity of the crystallographic components of PbSe and PbS semiconductors. However, a boundary is noted in PbSe/PbS CQD with a shell width >3 nm (panel b). A representative TEM image of CQDs shown in panel a is presented in panel c, exhibiting a size uniformity of ~5%. A representative SAED of CQDs shown in panel c is shown in panel d, confirming a rock-salt crystallographic structure ($Fm\bar{3}m$ space group). Similar rock-salt structures appeared in all of the investigated samples. The Pb/S/Se atomic ratios within the heterostructures, as measured by EDAX, ICP-AES, or/and XPS analysis of the investigated samples with different size and composition, core radius, r_{core}, and overall core/shell radius, r_{total}, are listed in Table 1. Representative EDAX and XPS spectra are supplied in the Supporting Information, Figure S1.

Representative absorption (dashed lines) and cw-PL (solid lines) spectra of a few samples with various composition and size, measured at room temperature (RT), are shown in Figure 1e. The bottom and top curves correspond to the spectra of PbSe core CQDs with average radius of r_{core} = 1.5 and 2.4 nm, respectively. The middle curves represent different heterostructures (c/sh, c/a-sh, and a-c/a-sh), with composition and size as labeled in the panel, when r_{core} = 1.5 nm and r_{total} is up to 2.4 nm. These sets of curves suggest the occurrence of a red-shift of the absorption and emission spectra of the heterostructures with respect to those of the primary cores with r_{core} = 1.5 nm, but they are blue-shifted with respect to that of pure PbSe cores with r_{core} = 2.4 nm. This midway shift is related to a quantum size effect combined with a composition tuning of the band edge energy. The experimental band gap energy, estimated by the first excitonic absorption band, and the corresponding calculated values (discussed below) of the studied materials are listed in Table 1. The table also designates the PL QY of a few selected samples. The determination of the QY is given in detail in the Supporting Information. Systematic improvement (up to 88%) of the QY was found in c/sh, c/a-sh, and a-c/a-sh CQDs *versus* the primary core CQDs. The relatively high QY might be related to the improved quality of surfaces, *e.g.*, close crystallographic match between PbSe core and PbS or $PbSe_xS_{1-x}$ shell, as well as the increase of the S% at the exterior surface, with a lower oxidation outcome. The cw-PL spectra shown in Figure 1e were pumped by a nonresonant excitation (1.54 eV), showing an asymmetric or a split band, Stokes shifted with respect to the first absorption band by an energy, E_s, as listed in Table 1, and Figure S2 in the Supporting Information. The nonresonant Stokes shift has an interesting behavior: (i) a reduction of E_s in c/sh heterostructures with respect to their primary cores. The Stokes shift is related to a total growth of r_{total} with respect to r_{core}, as well as to the generation of an exciton fine-structure by valley−valley and electron−hole exchange interactions. These interactions may be reduced in c/sh structures as the result of a *quasi*-type-II band alignment, as will be discussed below; (ii) E_s in c/a-sh and a-c/a-sh CQDs is smaller than in the corresponding cores but larger than that in core or c/sh CQDs of an equivalent size (see Table 1). Similar increase of E_s in alloyed CQDs (in comparison with pure cores) was observed before in II−VI[53,54] and III−V[55] quantum dots and was associated with a nonlinear effect such as optical bowing, induced by a lattice constant deformation or different carriers' distribution in alloyed materials.[54]

Figure 2 illustrates the evolution of the cw-PL spectra of a few samples, excited at 1.54 eV and recorded at different temperatures from 1.4 to 300 K as shown by the ruler in the figure. Panels a and e represent the spectra of reference PbSe cores, with an average radius, r_{core} = 1.5 and 2.4 nm, respectively. The cw-PL spectra correspond to a band edge exciton recombination emission at the L-point of the Brillouin zone of a PbSe semiconductor. Panels b and c show the spectra of PbSe/PbS c/sh and PbSe/$PbSe_{0.68}S_{0.32}$ c/a-sh CQDs, respectively, both with r_{core} = 1.5 nm and r_{total} = 2.1 nm. Panel d exhibits the spectra of $PbSe_{0.5}S_{0.5}$/$PbSe_{0.27}S_{0.73}$ a-c/a-sh CQDs with r_{total} = 2.4 nm. Once again, at all temperatures the emission energy of the heterostructures shows a midway shift between the emission energy of small and large reference cores (panels a and e). The cw-PL spectra of the smallest PbSe core CQDs are dominated by a single exciton band over the entire temperature range, similar to the observation found in ref 52. However, the emission spectra of the larger PbSe cores

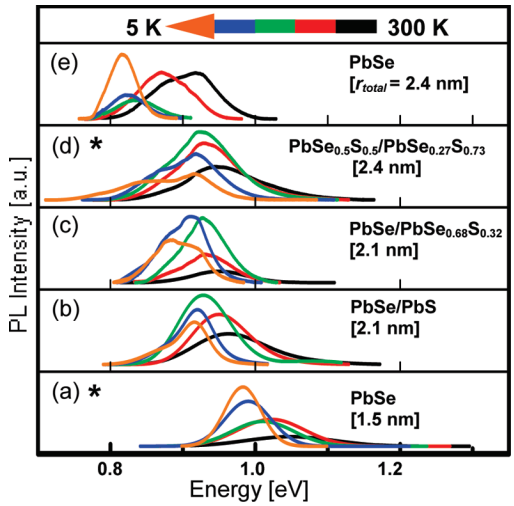

Figure 2. cw-PL spectra of PbSe core CQDs with core radius of (a) r_{core} = 1.5 nm and (e) r_{core} = 2.4 nm. cw-PL spectra of (b) PbSe/PbS core/shell and (c) $PbSe/PbSe_{0.68}S_{0.32}$ core/alloyed-shell CQDs, both with r_{core} = 1.5 nm and r_{total} = 2.1 nm. (d) cw-PL spectra of $PbSe_{0.5}S_{0.5}/PbSe_{0.27}S_{0.73}$ alloyed-core/alloyed-shell CQDs with r_{core} = 1.6 nm and r_{total} = 2.4 nm. The data were recorded at various temperatures shown by the ruler. (* indicates that the PL intensity was multiplied by a factor of 3 at RT).

occasionally exhibit a split band at elevated temperatures. The cw-PL spectra of the various heterostructures show an asymmetric or a split shape at all temperatures, presumably consisting of two overlapping emission bands, where the energy split is of the order 30−55 meV, decreasing with the increase of the shell width and the S/Se ratio (see Supporting Information, Figure S3). Interestingly, the split energy closely retains its value upon the increase in temperature, although the high energy component is gaining intensity with the increase in temperature. The splitting might be related to the occurrence of a recombination emission from two low lying excited states based on the following grounds: (i) a break of the 4-fold degeneracy at the Brillouin L-point minima in IV−VI rock-salt structures, by confinement or valley−valley interaction. Indeed, valley−valley interaction, previously reported,[56−58] suggested a split of the band edge into two manifolds, each composed of bright and dark states induced by exchange interaction. The valley−valley split energy is in the range of 20−60 meV, increasing with the decrease of the CQDs' size, close to the experimental values attained in this work, which also increased with the reduction of r_{total}; (ii) simultaneous emission from both dark and bright states, if a Boltzmann distribution at the cryogenic temperatures permits a heavy population of the higher energy bright state. This case is less probable, since the observed split of a few tenths of meV is substantially larger than a theoretical reported value for an exchange splitting between dark and bright states in pure PbSe cores; (iii) two emission processes can be related to parallel radiative recombination of a type-I and *quasi*-type-II transitions, overlapping in an ensemble of CQDs. Presumably, such a case can be excluded, based on the observed uniformity, size and composition; (iv) occurrence of energy transfer between subgroups of small and large CQDs. The examined CQDs were dissolved in glass solutions, with a relatively low concentration, minimizing the energy transfer process. Thus, valley−valley interaction is the most probable mechanism for a split emission band.

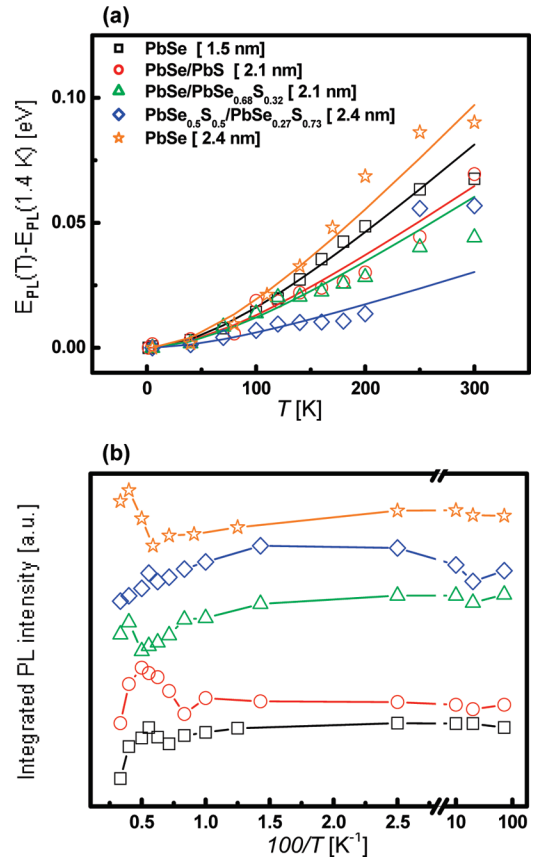

Figure 3. (a) Plot of the low cw-PL band emission peak energy relative to that at 1.4 K ($E_{PL}(T) - E_{PL}(1.4\ K)$) *versus* the temperature *T* of the samples mentioned in the legend. The symbols designate the experimental points, and the solid lines are the best fit curves. (b) Plot of the integrated PL intensity *versus* 100/*T* of the samples presented in panel a. The solid lines here are drawn to guide the eye.

Figure 3a displays the temperature variation of the peak emission of the low energy cw-PL band of a few heterostructures, large core and small reference core, as given in the legend. The figure demonstrates the peak energy at a temperature, *T*, relative to that at 1.4 K ($E_{PL}(T) - E_{PL}(1.4\ K)$) *versus* a temperature, *T*. The plots disclose a blue-shift of the emission energy with the increase in *T*, which is the biggest for the PbSe cores; however, they illustrate a moderate change in the heterostructures. The symbols designate the experimental points, and the solid lines are best fitted curves. A tangent line to the fitted curve evaluates the slope, revealing the temperature coefficient, d*E*/d*T*. This coefficient is most commonly derived from the temperature dependence of the first excitonic transition energy, using Varshni relation;[59,60] however, if the emission Stokes

TABLE 2. Energy Band-Gap Temperature Coefficient and Thermal Activation Energy of IV−VI CQDs' Heterostructures[a]

molecular formula of CQDs	r_{total} [nm]	dE/dT [meV/K]	ΔE_a [meV]
PbSe	1.5	0.32	15.51
PbSe/PbS	2.1	0.17	17.23
$PbSe/PbSe_{0.68}S_{0.32}$	2.1	0.15	15.51
$PbSe_{0.5}S_{0.5}/PbSe_{0.27}S_{0.73}$	2.4	0.06	
PbSe	2.4	0.48	21.54

bulk material	dE_g/dT [meV/K]
PbSe	0.51[62]
PbS	0.52[62]

[a]Energy band gap temperature coefficient, dE/dT; thermal activation energy, ΔE_a.

shift is invariant under the temperature, the coefficient derived in the present case should be relatively close to the band edge value, dE_g/dT. The best fitted coefficients of a few samples are listed in Table 2, indicating an increase of dE/dT with an increase in size[61] approaching the bulk value of dE_g/dT. Also, those coefficients of the heterostructures are reduced with respect to pure cores of equivalent r_{total}, which is most pronounced in a-c/a-sh CQDs. The temperature dependence of the coefficient dE_g/dT has dominant contributions from crystal dilation and electron−phonon interactions, as well as minor contributions from mechanical strain and thermal expansion of the wave function envelope.[61] Because the thermal expansion coefficients of bulk PbSe and PbS are almost identical,[62] it is expected that the electron−phonon coupling is the dominating effect responsible for the reduction of dE_g/dT in alloyed CQDs. A minor contribution might be also assigned to a reduction of a core/shell interface strain by a better crystallographic match. In any event, the low value of dE/dT in the alloyed CQDs suggests a thermal stability of the band edge properties, with a significant importance in various applications and in particular in solar energy panels.

Figure 3b demonstrates plots of the PL integrated intensity of the low energy cw-PL band *versus* 100/*T*. The plots show a similar tendency, including a plateau at the temperature range >10 to ~150 K, followed by low quenching of the intensity by an exciton−phonon interaction at higher temperatures, a typical behavior of a direct band gap semiconductor.[63] However, the trend is interrupted in two distinct points: (i) occurrence of an unusual climax in the intensity profile at a temperature between 150 and 250 K, appearing at higher temperature in c/sh and c/a-sh, compared with that of the primary cores, but with a very small effect in a-c/a-sh CQDs (see Supporting Information, Table S3). This abnormal climax was previously explained[52] as a thermal activation between dark and bright states, with activation energy (ΔE_a) close to the LO phonon energy ($LO_{(PbSe)}$ = 16.8 meV, $LO_{(PbS)}$ = 26 meV). The values of ΔE_a of the investigated samples are listed in Table 2, spanning a range that is in close agreement to the suggested theoretical values of the dark−bright splitting in pure PbSe cores;[56] (ii) an unexplained minor decrease of the intensity <10 K with an activation energy ~0.4 meV, way below the acoustic phonon energy (LA, TA ~4−6 meV).[64] It is worth noting that the best fit shown in panel a also shows some deviation from perfection at >150 K, in correlation with the abrupt climax shown in panel b, due to a change in the emission mechanism from a dark to a bright state emission.

The transient PL spectra were measured by exciting the sample with 1.17 eV and following the decay time (τ_{decay}) of the emission intensity. Figure 4a displays decay curves of the samples given in the legend, measured at RT, monitoring the low energy PL component. Predominantly, the curves exhibit a single exponent behavior, where the value of τ_{decay} decreases upon the growth of a core radius from r_{core} = 1.5 to 2.4 nm. However, the τ_{decay} of the c/sh CQDs is longer than that of the primary PbSe cores. Plots of the values of τ_{decay} measured at various temperatures (as indicated by the arrow), monitored across the PL spectrum of PbSe cores and PbSe/PbS c/sh CQDs, are shown in the inset of Figure 4a. The symbols are the experimental points, and the solid lines are to guide the eye. It shows that the τ_{decay} of the core CQDs is approximately invariant across the PL spectrum. However, there is a pronounced decrease of the τ_{decay} when moving from the red to the blue side of a PL spectra of a c/sh sample, mainly pronounced at low *T* but becoming insensitive to the detection energy at RT. The variation of τ_{decay} across the PL band supports the existence of emission of at least two manifold of states in the PL spectrum of the heterostructures, involving different radiative transitions, each of which having a distinct dependence on the temperature.

τ_{decay} is correlated to the PL radiative lifetime (τ_{rad}) by the relation, $\tau_{rad} = \tau_{decay}/QY$ (QY values are given in Table 1). Considering this relation, Figure 4b represents plots of τ_{rad} *versus* the measured *T* of the samples given in the legend of panel a, monitored only on the low energy PL component. These plots reveal a drastic decrease of τ_{rad} with the increase in *T* in core and c/sh CQDs, related to a dark exciton emission[52] but only a minor change in c/a-sh and a-c/a-sh CQDs. The small variation of τ_{rad} in the later CQDs is also related to the diminished climax in the PL intensity *versus* 1/*T* (see Figure 3b). Both effects suggests elevation of the dark exciton characteristic in alloyed CQDs. Figure 4c compares plots of τ_{rad} *versus* r_{total} of core and c/sh CQDs at three different *T* (5, 100, and 300 K). These curves reflect a common behavior, characterized by a reduction that is turned into an extension of τ_{rad} with the increase in r_{total} (called bowing effect). The turning points are mainly pronounced when measured at low *T*. It is important to note that the decay processes in c/a-sh samples resemble those of the c/sh materials (not shown), but

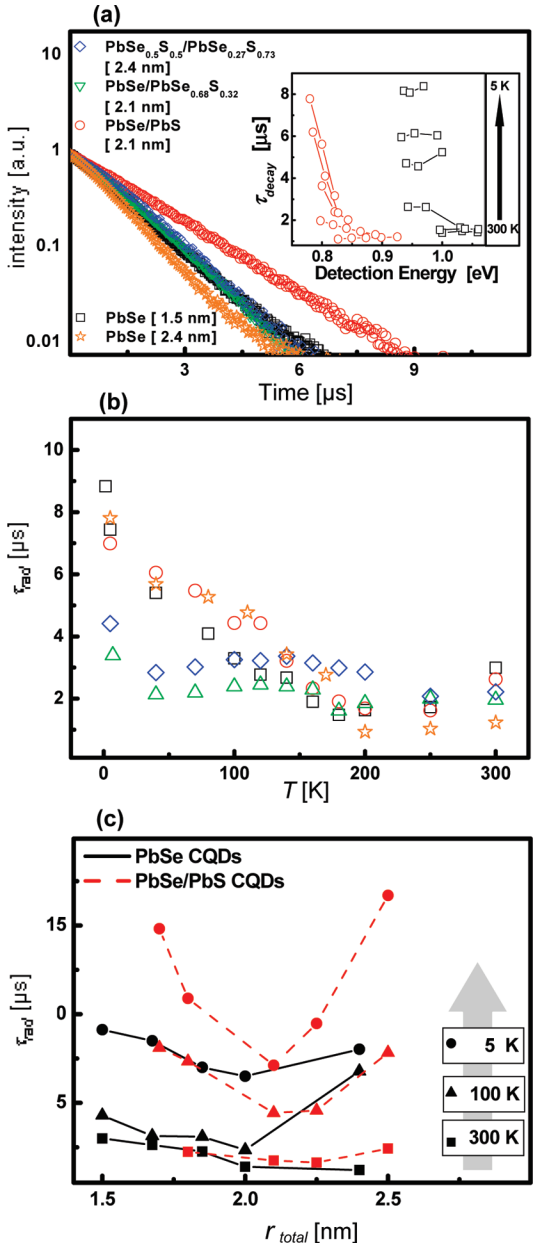

Figure 4. (a) Representative PL decay curves of the samples listed in the legend at RT. The inset in panel a presents plots of the measured decay time, τ_{decay}, *versus* the detection energy across the PL spectrum of core and core/shell CQDs, measured at different temperatures (5−300 K) as indicated by the arrow. (b) Variation of the radiative lifetime *versus* the temperature of the samples listed in panel a. (c) Plots of the radiative lifetime *versus* the radius (r_{total}) of cores (solid line) and the corresponding core/shell (dashed line) CQDs, measured at the various temperatures as indicated in the figure.

the turning points in c/sh and c/a-sh CQDs occur at a smaller r_{total} than that of cores of equivalent size. In fact, a turning point in the variation of τ_{rad} with size was already reported in PbSe core CQDs at RT for samples with r_{core} between 2 to 10 nm.[56−65] Currently the mechanism of this behavior is not clearly understood; however it was previously suggested[65] that the initial reduction of τ_{rad} with increasing size could be attributed to the size-dependence of the matrix element for spontaneous emission $|\langle\psi_f|\hat{\mathbf{p}}|\psi_i\rangle|^2$ that governs the recombination rate up to $r_{total} \approx 2$ nm.[66] For larger sizes, however, the matrix element is expected to become size-independent, so τ_{rad} becomes proportional to the wavelength of emitted radiation, which is consistent with the trend observed in Figure 4c.

The electronic structure of PbSe/PbS c/sh and PbSe/$PbSe_xS_{1-x}$ c/a-sh CQDs was calculated using the $k \cdot p$ envelope function method using a four-band bulk Hamiltonian and band edge Bloch functions.[67] The Hamiltonian was adjusted to the discontinuity at the PbSe/PbS interface by the appropriate choice of the kinetic energy term, ensuring probability current conservation and continuity of the envelope functions (see Supporting Information). In addition, the Hamiltonian potential energy term included the heterostructure band offset, abrupt for the c/sh structure but considered as a smooth function for the c/a-sh CQDs.[68] Presumably, the smooth potential profile reflects the nature of the interface region in alloyed materials with gradient composition, being an extension of the standard treatment for semiconductor heterostructures. The overall band offset was chosen as that of the corresponding bulk PbSe and PbS materials (where the valence band maximum of bulk PbS lies 0.025 eV above that of PbSe, while the conduction band minimum lies 0.155 eV above that of PbSe).[51,67] Diagonalization of the envelope function Hamiltonian yielded the electron and hole wave functions, as well as a good approximation of the energy values of the conduction and valence-band's states. Representative radial distribution functions, $|\psi(r)|^2r^2$, of the holes and electrons of a few samples are shown in Supporting Information, Figure S3. Three-dimensional plots of the electron and hole distribution functions on (111) cut-plane for a pure core (panel a), c/sh CQDs (panels b and c), and c/a-sh (panels d and e) of equivalent r_{total} are shown in Figure 5. Panels f and g show the electron and the hole distribution for a c/a-sh with $r_{core} = 3$ nm and $r_{total} = 5$ nm. In the case of a pure core structure, the distribution of electron and hole is virtually identical, and thus panel a describes either one of the carriers. The choice of the (111) plane is made for the calculation convenience only and is equivalent to choosing any other crystallographic plane for the distribution representation, since the ground state wave functions are spherically symmetric. These plots reveal a distinct trend, in which the lowest energy hole state, $|1/2, 1\rangle$ (1/2 denotes the total angular momentum j of the state, and ± 1 corresponds to the parity π), is more delocalized with respect to its counter partner, the lowest energy electron state $|1/2, -1\rangle$, in c/sh and c/a-sh CQDs, characteristic of *quasi*-type-II configuration at the band edge. This electronic distribution explains the experimental observations of the gradual red-shift of the absorption spectra with the increase of the shell width. The electron and hole spa-

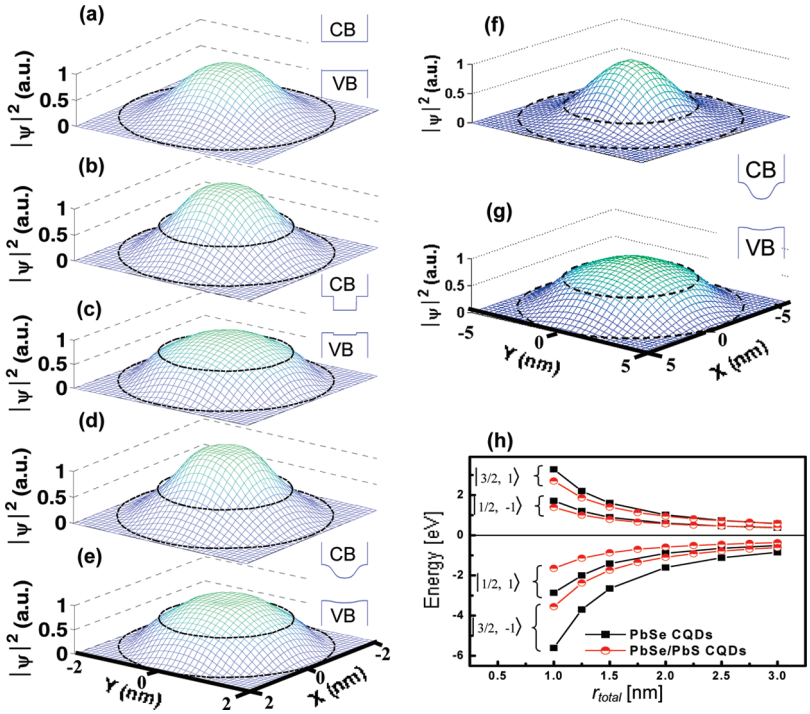

Figure 5. Probability density on the (111) cut-plane for electron and hole in (a) PbSe CQDs, $r_{total} = 2.4$ nm. (b) Electron and (c) hole in PbSe/PbS CQDs, $r_{core} = 1.5$ nm, $r_{total} = 2.3$ nm. (d) Electron and (e) hole in c/a-sh CQDs, $r_{core} = 1.6$ nm, $r_{total} = 2.4$ nm. (f) Electron and (g) hole in c/a-sh CQDs, $r_{core} = 3$ nm, $r_{total} = 5$ nm (Both dashed circles, outer and inner, represent the external particle boundary and the core/shell interface location, respectively.) The insets marked VB (valence band) and CB (conduction band) schematically represent the radial potential energy profile used in the calculation in each case. (h) Energy as a function of r_{total} of two lowest states of electron and hole in PbSe core and PbSe/PbS core/shell CQDs with $r_{total}/r_{core} = 3/2$.

tial distribution functions in c/sh CQDs shown in Figure 5, panels b and c suggest that the distribution of both carriers is similar to that of a c/a-sh structure (Figure 5, panels d and e); however, the distribution differs from the case of a simple core CQD of comparable total size (Figure 5a). The calculations show that for heterostructured particles with $r_{core} < 3$ nm the energies of the lowest lying electron levels exceed the potential barrier height (either abrupt or gradual), located at the interface between the core and the shell, thus significantly reducing the effect of quantum confinement induced by the shell layer. On the other hand, in the case of larger c/sh or c/a-sh particles the electron energy is lower than the barrier height, thus enforcing the confinement (and subsequently the localization) of the electron in the core region (cf. Figure 5, panels b and f). However, the energy difference between the valence band edges of PbSe and PbS is almost an order of magnitude smaller than that between the conduction band edges, and hence the hole distribution is influenced by the shell to a much lesser extent (*cf.* Figure 5, panels c and g).

Figure 5h displays the calculated energy of two lowest energy states *versus* the r_{total} of core and c/sh CQDs with $r_{total}/r_{core} = 3/2$. This figure reveals a pronounced influence of the shell on the energy levels of the carriers. In the case of a c/sh structure, both the electron and hole levels are lowered in energy relative to a core structure of the same size, with a larger influence on the hole levels. In the framework of this model the energy levels of c/a-sh structures are almost identical to those of c/sh and hence are not shown here. This finding is consistent with the experimental observation of the red-shift in the emission energy of the c/sh and c/a-sh heterostructures, relative to the cores of corresponding size. The theoretical $|1/2, 1\rangle \rightarrow |1/2, -1\rangle$ transition energies (which is the first excitonic transition) are listed in Table 1 and are compared with the experimental absorption band edge energies, with a close agreement for CQDs with $r_{total} > 1.5$ nm (Apparently, the accuracy of the model is not satisfactory for very small sizes due to the breakdown of the major assumption that the envelope function is slowly varying on the scale of the unit cell). The model reproduced the band edge energies of the CQDs with relatively close agreement with the experiment, as well as predicted varying delocalization extent of the electrons in the lowest conduction band. The explanation of the reported variation of various physical properties of c/sh and c/a-sh heterostructures would demand further theoretical considerations (*e.g.*, mass anisotropy, exchange interactions), which are beyond the scope of the discussed model but will be done in the future.

CONCLUSION

In conclusion, the current work investigated the optical properties of PbSe/PbS c/sh, PbSe/$PbSe_xS_{1-x}$ c/a-sh, and $PbSe_yS_{1-y}$/$PbSe_xS_{1-x}$ a-c/a-sh CQDs over a wide

range of temperatures. The investigated heterostructures have distinguished properties in comparison with those of pure PbSe core CQDs with equivalent overall size (r_{total}) and identical core radius (r_{core}): (i) increase of the PL QY at RT with respect to their primary core CQDs; (ii) red-shift of the emission energy with respect to primary cores, but a blue-shift in comparison with a simple core of similar overall size, revealing composition-tunable band gap energy; (iii) split of the PL exciton band, at all temperatures, presumably due to a valley−valley interaction, when the split energy is reduced with the increase of the shell width (or r_{total}); (iv) smaller band edge temperature coefficient (especially at alloyed CQDs) with respect to the primary cores, suggesting a thermal stability; (v) drastic change in lifetime between low and high temperatures in c/sh CQDs, but only a minor change in the alloyed CQDs. This invariant lifetime is also correlated with a minor dark−bright thermal activation process in the alloyed heterostructures, both properties suggesting elevation of the dark characteristic upon the induction of gradient composition with a soft core−shell interface; (vi) bowing variation of the radiative lifetime with the overall size, r_{total}, with a turn point that deviates from that of a simple cores of equivalent size. The unique behavior of the c/sh, c/a-sh, and a-c/a-sh are related to the relatively good crystal match between the core and shell constituents, the specific composition, and the partial delocalization of at least one of the carriers (in the framework of this investigation, the delocalization of the hole) over the entire structure. A smooth potential at the core−shell interface was applied here, for the first time, for the determination of the electronic structure of alloyed IV−VI CQDs, showing similar behavior for the electron and hole wave function in c/a-sh and c/sh heterostructures. The explanation for the reported variation of various physical properties of c/sh and c/a-sh heterostructures would demand further theoretical considerations that are beyond the scope of the discussed model and will be done in the future. The heterostructuring and composition control of the discussed samples could be of significant importance in applications where the CQDs' size is restricted, *e.g.*, biological markers or self-assembled CQDs in optoelectronic devices, while at the same time there are stringent demands regarding the optical tunability.

METHODS

The synthesis of PbSe cores, PbSe/PbS c/sh, PbSe/PbSe$_x$S$_{1-x}$ core/a-sh, and PbSe$_x$S$_{1-x}$/PbSe$_y$S$_{1-y}$ ($0< x, y <1$) a-c/a-sh CQDs, all coated with oleic acid ligands, is described in detail elsewhere.[21,22] However, for completeness of presentation, a brief description is given here. PbSe CQDs were formed by injection of Pb and Se precursors, Pb(acetate)$_2$ and TOP:Se, into a preheated mother solution, composed of oleic acid (OA), trioctyl phosphine (TOP), and phenyl-ether. It should be noted that alternative precursors were tried, including PbO as the lead ion source and octadecene[69] as a noncoordinating solvent; however, these starting materials led to a faster reaction, eliminating attaining small CQDs, so the alternative precursors were not used in the current study. The PbSe/PbS core/shell CQDs were prepared in two pots, starting with a preliminary synthesis of PbSe cores, their separation from the original pot and resuspension in a Se free solution. The following stage involves an epitaxial coating of PbS shells in a second pot, by the injection of the stoichiometric amounts of Pb and S ions into the core solution. PbSe/PbSe$_x$S$_{1-x}$ and PbSe$_x$S$_{1-x}$/PbSe$_y$S$_{1-y}$ CQDs are produced in one pot by simultaneous injections of Pb, Se, and S precursors, Pb(acetate)$_2$, TOP:Se and TOP:S, into the preliminary mother solution. Examination of intermediate aliquots by EDAX, ICP-AES, or/and XPS revealed the creation of embryonic PbSe or PbSe$_y$S$_{1-y}$ nuclei (measured <0.5 min after the injection) and a delayed precipitation of PbSe$_x$S$_{1-x}$ shells. A preliminary injection of Pb/Se/S ions ratio of 1/1/0.5 led to the nucleation of a pure PbSe core due to the faster reactivity of the Se precursors at the nucleation stage.[21] However, the increase of the S/Se ratio (S/Se > 1.5/1) enabled an immediate integration of both elements with the nuclei (monitored already in the first aliquot). Further aliquots revealed a gradient increase of the S/Se ratio when moving from the interface toward the exterior surface. For simplicity, the samples were labeled as PbSe$_y$S$_{1-y}$/PbSe$_x$S$_{1-x}$.

The oleate-capped PbSe CQDs were stored either in a chloroform solution or as a dry powder in air or in nitrogen ambient. The stability of these CQDs was examined over a period of time by recording the absorption spectra and following the consistency of the low exciton energy. Plots of this exciton energy *versus* time suggest that the exciton energy in the core samples is blue-shifted by ~400 meV over a period of days for the CQDs kept in a chloroform solution. Such a blue-shift, however, occurs over months for the samples kept as dry powders. On the other hand, the energy shift is smaller for the PbSe/PbS c/sh samples and even nearly disappeared for the CQDs coated with three PbS shell monolayers. It is presumed that the exciton energy blue-shift is due to oxidation of the surface and a decrease of the effective size of the core.[22,23] Obviously, the penetration of oxygen through the PbS shell is reduced with the growth of the shell width. Furthermore, storage of the CQDs in a nitrogen environment nearly eliminates any spectral drift over a period of months, even extending to 2−3 years. Also, the studied samples showed photostability when exposed to visible (514.5 nm Ar+ or 800 nm Ti:sapphire lasers) and near-infrared (1400−1500 nm diode laser) radiation over weeks. It should be noted that most of the optical measurements were carried out at cryogenic temperatures (see below), inducing a He gas environment around the samples. Unpublished results determined degradation of the samples when exposed to intense pulsed UV radiation, which is avoided completely in the current study.

The morphology and crystallography of the colloidal CQDs were examined by X-ray diffraction, transmission electron microscopy (TEM model Tecnai T20), high-resolution TEM (HR-TEM), and selected area electron diffraction (JEOL 3010). The TEM specimens were prepared by injecting small liquid droplets of the solution on a copper grid (300 mesh) coated with amorphous carbon film and then dried at room temperature.

The absorption spectra of the samples were recorded on a JASCO V-570 UV−vis−NIR spectrometer. The cw-PL spectra were obtained by exciting the samples with a tunable Ti:sapphire laser, Coherent 890 (E_{exc} = 1.48−1.80 eV). The PL spectra of the materials studied were recorded at a temperature range of 1.4−300 K, while immersing the samples in a variable temperature Janis cryostat and detecting the emission with an Acton Spectrapro 2300i monochromator, which was equipped with a cooled InGaAs CCD. The PL decay curves were recorded by exciting the samples with a Nd:YAG laser, Continum Minilite II (E_{exc} = 1.17 eV). The measurements utilized a laser flux <0.1 mJ/cm^2, corresponding to a photon fluence of $j_p \approx 10^{11}$ photons/cm^2 per pulse. Considering the absorption cross-section of $\sigma_0 \approx 10^{-15}$ cm^2, measured in ref 16, the number of photogenerated

excitons is given by $\langle N_0 \rangle = j_p \sigma_0$ and estimated to be $10^{-4} \ll 1$, ensuring the generation of single excitons. The cw-PL and transient-PL curves were monitored by a photon multiplier tube, Hamamatsu NIR-PMT H10330-75. The PL QY was measured utilizing integrating sphere technique described by Friend *et al.*[52,70]

Acknowledgment. The authors thank G. Kventsel for helpful discussions, providing many insightful comments, A. Bartnik and F. Wise for helpful discussions and guidance on the theoretical model, A. Efros for the useful scientific discussions, G. Grinbom for her assistance with the TEM measurements, and O. Solomeshch for assistance in the quantum yield measurements. The authors acknowledge support from the Israel Science Foundation (Projects No. 1009/07 and No. 1425/04), the USA-Israel Binational Science Foundation (No. 2006-225), and the Ministry of Science (No. 3-896).

Supporting Information Available: EDAX and XPS data, Stokes shift, Gaussian curve fit to the PL spectra of representative samples, determination of the QY, and the description of the theoretical model. This material is available free of charge *via* the Internet at http://pubs.acs.org.

REFERENCES AND NOTES

1. Steigerwald, M. L.; Brus, L. E. Semiconductor Crystallites: A Class of Large Molecules. *Acc. Chem. Res.* **1990**, *23*, 183–188.
2. Peng, X.; Manna, L.; Yang, W.; Wickham, J.; Scher, E.; Kadavanich, A.; Alivisatos, A. P. Shape Control of CdSe Nanocrystals. *Nature* **2000**, *404*, 59–61.
3. Akamatsu, K.; Tsuruoka, T.; Nawafune, H. Band Gap Engineering of CdTe Nanocrystals through Chemical Surface Modification. *J. Am. Chem. Soc.* **2005**, *127*, 1634–1635.
4. Ripmeester, J. A.; Yu, K. Gradiently Alloyed $Zn_xCd_{1-x}S$ Colloidal Photoluminescent Quantum Dots Synthesized via a Noninjection One-pot Approach. *J. Phys. Chem. C* **2008**, *112*, 4908–4919.
5. Ma, W.; Luther, J. M.; Zheng, H.; Wu, Y.; Alivisatos, A. P. Photovoltaic Devices Employing Ternary PbS_xSe_{1-x} Nanocrystals. *Nano Lett.* **2009**, *9*, 2072–2077.
6. Bailey, R. E.; Nie, S. M. Alloyed Semiconductor Quantum Dots: Tuning the Optical Properties without Changing the Particle Size. *J. Am. Chem. Soc.* **2003**, *125*, 7100–7106.
7. Piven, N.; Susha, A. S.; Doeblinger, M.; Rogach, A. L. Aqueous Synthesis of Alloyed $CdSe_xTe_{1-x}$ Nanocrystals. *J. Phys. Chem. C* **2008**, *112*, 15253–15259.
8. Erwin, S. C.; Zu, L.; Haftel, M. I.; Efros, A. L.; Kennedy, T. A.; Norris, D. J. Doping Semiconductor Nanocrystals. *Nature* **2005**, *436*, 91–94.
9. Schooss, D.; Mews, A.; Eychmüller, A.; Weller, H. Quantum-Dot Quantum-Well CdS/HgS/CdS: Theory and Experiment. *Phys. Rev. B* **1994**, *49*, 17072–17078.
10. Danek, M.; Jensen, K. F.; Murray, C. B.; Bawendi, M. G. Synthesis of Luminescent Thin-Film CdSe/ZnSe Quantum Dot Composites Using CdSe Quantum Dots Passivated with an Overlayer of ZnSe. *Chem. Mater.* **1996**, *8*, 173–180.
11. Ivanov, S. A.; Piryatinski, A.; Nanda, J.; Tretiak, S.; Zavadil, K.; Walalce, W. O.; Werder, D.; Klimov, V. I. Type-II Core/Shell CdS/ZnSe Nanocrystals: Synthesis, Electronic Structures, and Spectroscopic Properties. *J. Am. Chem. Soc.* **2007**, *129*, 11708–11719.
12. Piryatinski, A.; Ivanov, S. A.; Tretiak, S.; Klimov, V. I. Effect of Quantum and Dielectric Confinement on the Exciton-Exciton Interaction Energy in Type-II Core/Shell Semiconductor Nanocrystals. *Nano Lett.* **2007**, *7*, 108–115.
13. Oron, D.; Kazes, M.; Banin, U. Multiexitons in Type-II Colloidal Semiconductor Quantum Dots. *Phys. Rev. B* **2007**, *75*, 035330.
14. Mamutin, V. V.; Egorov, A. Yu.; Kryzhanovskaya, N. V. Molecular Beam Epitaxy Growth Methods of Wavelength Control for InAs/(In)GaAsN/GaAs Heterostructures. *Nanotechnology* **2008**, *19*, 445715.
15. Lauhon, L. J.; Gudiksen, M. S.; Wang, D.; Lieber, Ch. M. Epitaxial Core-Shell and Core Multishell Nanowire Heterostructures. *Nature* **2002**, *420*, 57–61.
16. Dorfs, D.; Salant, A.; Popov, I.; Banin, U. ZnSe Quantum Dots With in CdS Nanorods: A Seeded Growth Type-II System. *Small* **2008**, *4*, 1319–1323.
17. Nonoguchi, Y.; Nakashima, T.; Kawai, T. Tuning Band Offsets of Core/Shell CdS/CdTe Nanocrystals. *Small* **2009**, *5*, 2403–2406.
18. Smith, A. M.; Mohs, A. M. Nie, Sh. Tuning the Optical and Electronic Properties of Colloidal Nanocrystals by Lattice Strain. *Nat. Nanotechnol.* **2009**, *4*, 56–63.
19. Klimov, V. I.; Ivanov, S. A.; Nanda, J.; Achermann, M.; Bezel, I.; J. McGuire, A.; Piryatinski, A. Single-Exciton Optical Gain in Semiconductor Nanocrystals. *Nature* **2007**, *447*, 441–446.
20. Sashchiuk, A.; Langof, L.; Chaim, R.; Lifshitz, E. Synthesis and Characterization of PbSe and PbSe/PbS Core-Shell Colloidal Nanocrystals. *J. Cryst. Growth* **2002**, *240*, 431–438.
21. Brumer, M.; Kigel, A.; Amirav, L.; Sashchiuk, A.; Solomesch, O.; Tessler, N. Lifshitz, E.PbSe/PbS and $PbSe/PbSe_xS_{1-x}$ Core/Shell Nanocrystals. *Adv. Funct. Mater.* **2005**, *15*, 1111–1116.
22. Lifshitz, E.; Brumer, M.; Kigel, A.; Sashchiuk, A.; Bashouti, M.; Sirota, M.; Galun, E.; Burshtein, Z.; Le Quang, A. Q.; Ledoux-Rak, I.; et al. Air-Stable PbSe/PbS and $PbSe/PbSe_xS_{1-x}$ Core-Shell Nanocrystals Quantum Dots and Their Applications. *J. Phys. Chem. B* **2006**, *110*, 25356–25365.
23. Stouwdam, J. W.; Shan, J.; van Veggel, F. C. J. M. Photostability of Colloidal PbSe and PbSe/PbS Core/Shell Nanocrystals in Solution and in the Solid State. *J. Phys. Chem. C* **2007**, *111*, 1086–1092.
24. Xu, J.; Cui, D.; Zhu, T.; Paradee, G.; Liang, Z.; Wang, Q.; Xu, Sh.; Wang, A. Y. Synthesis and Surface Modification of PbSe/PbS Core-Shell Nanocrystals for Potential Device Applications. *Nanotechnology* **2006**, *17*, 5428–5434.
25. Pietryga, J. M.; Werder, D. J.; Williams, D. J.; Casson, J. L.; Schaller, R. D.; Klimov, V. I.; Hollingsworth, J. A. Utilizing the Lability of Lead Selenide To Produce Heterostructured Nanocrystals with Bright, Stable Infrared Emission. *J. Am. Chem. Soc.* **2008**, *130*, 4879–4885.
26. Klimov, V. I.; Mikhailovsky, A. A.; Xu, S.; Malko, A.; Hollingsworth, J. A.; Leatherdale, C. A.; Eisler, H. J.; Bawendi, M. G. Optical Gain and Stimulated Emission in Nanocrystal Quantum Dots. *Science* **2000**, *290*, 314–317.
27. Choudhury, K. R.; Sahoo, Y.; Jang, S.; Prasad, P. N. Efficient Photosensitization and High Optical Gain in a Novel Quantum-Dot-Sensitized Hybrid Photorefractive Nanocomposite at a Telecommunications Wavelength. *Adv. Func. Mater.* **2005**, *15*, 751–756.
28. Nozik, A. J. Nanosicence and Nanostructures for Photovoltaic and Solar Fuels. *Nano Lett.* **2010**, *10*, 2735–2741.
29. Nozik, A. J. Quantum Dot Solar Cells. *Phys. E (Amsterdam, Neth.)* **2002**, *14*, 115–120.
30. Lee, H.; Wang, M. K.; Chen, P.; Gamelin, D. R.; Zakeeruddin, S. M.; Graetzel, M; Nazeeruddin, M. K. Efficient CdSe Quantum Dot-Sensitized Solar Cells Prepared by an Improved Successive Ionic Layer Adsorption and Reaction Process. *Nano Lett.* **2009**, *9*, 4221–4227.
31. Bang, H.; Kamat, P. V. Quantum Dot Sensitized Solar Cells. CdTe versus CdSe Nanocrystals. *ACS Nano* **2009**, *3*, 1467–1476.
32. Noone, K. M.; Munro, A. M.; Anderson, N. C.; Horwitz, N.; Kulkarni, A. P.; Ginger, D. S. Absence of Long-Lived Photoinduced Charge Transfer in Blends of PbSe Quantum Dots and Conjugated Polymers. *ACS Nano* **2009**, *3*, 1345–1352.
33. Fischbein, M. D.; Puster, M.; Drndic, M. Monolayer Suppression of Transport Imaged in Annealed PbSe Nanocrystal Arrays. *Nano Lett.* **2010**, *10*, 2155–2161.
34. Sargent, E. H. Infrared Photovoltaics Made by Solution Processing. *Nat. Photonics* **2009**, *3*, 325–331.
35. Loss, D.; DiVincenzo, D. P. Quantum Computation with Quantum Dots. *Phys. Rev. A* **1998**, *57*, 120–126.

36. Petta, J. R; Johnson, A. C.; Taylor, J. M.; Laird, E. A.; Yacoby, A.; Lukin, M. D.; Marcus, C. M; Hanson, M. P.; Gossard, A. C. Coherent Manipulation of Coupled Electron Spins in Semiconductor Quantum Dots. *Science* **2005**, *309*, 2180–2184.
37. Dubertret, B. Quantum Dots−DNA Detectives. *Nat. Mater.* **2005**, *4*, 797–798.
38. Smith, A. M.; Nie, S. Next-Generation Quantum Dots. *Nat. Biotechnol.* **2009**, *27*, 732–733.
39. Alivisatos, P. The Use of Nanocrystals in Biological Detection. *Nat. Biotechnol.* **2004**, *22*, 47–52.
40. Tang, J.; Hinds, S.; Kelley, S. O.; Sargent, E. H. Synthesis of Colloidal $CuGaSe_2$, $CuInSe_2$, and $Cu(InGa)Se_2$ Nanoparticles. *Chem. Mater.* **2008**, *20*, 6906–6910.
41. Fradkin, L.; Langof, L.; Lifshitz, E.; Rogach, A.; Gaponik, N.; Weller, H.; Eychmüller, A. Magneto-Optical Studies of $HgTe/Hg_xCd_{1-x}Te$(S) Core-Shell Nanocrystals. *ChemPhysChem* **2003**, *4*, 1203–1210.
42. Qian, H.; Dong, C.; Peng, J.; Qiu, X.; Xu, Y.; Ren, J. High-Quality and Water-Soluble Near-Infrared Photoluminescent CdHgTe/CdS Quantum Dots Prepared by Adjusting Size and Composition. *J. Phys. Chem. C* **2007**, *111*, 16852–16857.
43. Tsay, J. M.; Pflughoefft, M.; Bentolila, L. A.; Weiss, S. Hybrid Approach to the Synthesis of Highly Luminescent CdTe/ZnS and CdHgTe/ZnS Nanocrystals. *J. Am. Chem. Soc.* **2004**, *126*, 1926–1927.
44. Zhong, X. H.; Han, M. Y.; Dong, Z. L.; White, T. J.; Knoll, W. Composition-Tunable $Zn_xCd_{1-x}Se$ Nanocrystals With High Luminescence and Stability. *J. Am. Chem. Soc.* **2003**, *125*, 8589–8590.
45. Wang, F.; Ren, X.; Kahen, K.; Hahn, M. A.; Rajeswaran, M.; Maccagnano-Zacher, S.; Silcox, J.; Cragg, G. E.; Efros, A.; Krauss, T. D. Non-Blinking Semiconductor Nanocrystals. *Nature* **2009**, *459*, 686–689.
46. Li, L.; Daou, T. J.; Texier, I.; Thi Kim Chi, T.; Quang Liem, N.; Reiss, P. Highly Luminescent $CuInS_2$/ZnS Core/Shell Nanocrystals: Cadmium-Free Quantum Dots for in Vivo Imaging. *Chem. Mater.* **2009**, *21*, 2422–2429.
47. Osovsky, R.; Cheskis, D.; Kloper, V.; Sashchiuk, A.; Kroner, M.; Lifshitz, E. Continuous-Wave Pumping of Multiexcitons in Single Blinking Free Colloidal Quantum Dots. *Phys. Rev. Lett.* **2009**, *102*, 197401.
48. Kloper, V.; Osovsky, R.; Cheskis, D.; Sashchiuk, A.; Lifshitz, E. Suppressed Blinking CdTe/CdSe Core-Shell Quantum Dots. *Phys. Status Solidi C* **2009**, *6*, 2719–2721.
49. Krauss, T. D.; Peterson, J. J. Bright Future for Fluorescence Blinking in Semiconductor Nanocrystals. *J. Phys. Chem. Lett.* **2010**, *1*, 1377–1382.
50. Montazeri, M.; Fickenscher, M.; Smith, L. M.; Jackson, H. E.; Rice, J. Y.; Kang, J. H.; Gao, Q.; Tan, H. H.; Jagadish, Ch.; Guo, Y.; et al. Direct Measure of Strain and Electronic Structure in GaAs/GaP Core-Shell Nanowires. *Nano Lett.* **2010**, *10*, 880–886.
51. Bartnik, A. C.; Wise, F. W.; Kigel, A.; Lifshitz, E. Electronic Structure of PbSe/PbS Core-Shell Quantum Dots. *Phys. Rev. B* **2007**, *75*, 245424.
52. Kigel, A.; Brumer, M.; Maikov, G. I.; Sashchiuk, A.; Lifshitz, E. Thermal Activation of Photoluminescence in PbSe Nanocrystals. *Small* **2009**, *5*, 1675–1681.
53. Garrett, M. D.; Dukes, A. D.; McBride, J. R.; Smith, N. J.; Pennycook, S. J.; Rosenthal, S. J. Band Edge Recombination in CdSe, CdS and CdS_xSe_{1-x} Alloy Nanocrystals Observed by Ultrafast Fluorescence Upconversion: The Effect of Surface Trap States. *J. Phys. Chem. C.* **2008**, *112*, 12736–12746.
54. Bailey, R. E.; Nie, S. J. Alloyed Semiconductor Quantum Dots: Tuning the Optical Properties without Changing the Particle Size. *J. Am. Chem. Soc.* **2003**, *125*, 7100.
55. Huang, Y. H.; Cheng, F. L.; Chen, R. T.; Chen, Y. F.; Tsen, K. T. Studies of Stokes Shift in $In_xGa_{1-x}N$ Alloys. *J. Appl. Phys.* **2007**, *101*, 103521.
56. An, J. M.; Franceschetti, A.; Zunger, A. The Excitonic Exchange Splitting and Radiative Lifetime in PbSe Quantum Dots. *Nano Lett.* **2007**, *7*, 2129–2135.
57. Allan, A.; Delerue, C. Confinement Efects in PbSe Quantum Wells and Nanocrystals. *Phys. Rev. B* **2004**, *70*, 245321.
58. Harbold, J. M.; Wise, F. W. Photoluminescence Spectroscopy of PbSe Nanocrystals. *Phys. Rev. B* **2007**, *76*, 125304.
59. Turyanska, L.; Patane, A.; Henini, M.; Hennequin, B.; Thomas, N. R. Temperature Dependence of the Photoluminescence Emission from Thiol-Capped PbS Quantum Dots. *Appl. Phys. Lett.* **2007**, *90*, 101913.
60. Varshni, Y. P. Temperature Dependence of the Energy Gap in Semiconductors. *Physica* **1967**, *34*, 149–154.
61. Olkhovets, A.; Hsu, R.-C.; Lipovskii, A; Wise, F. W. Size-Dependent Temperature Variation of the Energy Gap in Lead-Salt Quantum Dots. *Phys. Rev. Lett.* **1998**, *81*, 3539–3542.
62. Madelung, O. *Semiconductors: Data Handbook*, 3rd ed.; Springer: New York, 2004.
63. Morello, G.; De Giorgi, M.; Kudera, S.; Manna, L.; Cingolani, R.; Anni, M. Temperature and Size Dependence of Nonradiative Relaxation and Exciton-Phonon Coupling in Colloidal CdTe Quantum Dots. *J. Phys. Chem. C* **2007**, *111*, 5846–5849.
64. Upadhyaya, K. S.; Yadav, M.; Upadhyaya, G. K. Lattice Dynamics of IV−VI Ionic Semiconductors: An Application to Lead Chalcogenides. *Phys. Status Solidi B* **2002**, *229*, 1129–1139.
65. Moreels, I.; Lambert, K.; Smeets, D.; De Muynck, D.; Nollet, T.; Martins, J. C.; Vanhaecke, F.; Vantomme, A.; Delerue, C.; Allan, G.; et al. Size-Dependent Optical Properties of Colloidal PbS Quantum Dots. *ACS Nano* **2009**, *3*, 3023–3030.
66. Van Driel, A. F.; Allan, G.; Delerue, C.; Lodahl, P.; Vos, W. L.; Vanmaekelbergh, D. Frequency-Dependent Spontaneous Emission Rate from CdSe and CdTe Nanocrystals: Influence of Dark States. *Phys. Rev. Lett.* **2005**, *95*, 236804.
67. Kang, I.; Wise, F. W. Electronic Structure and Optical Properties of PbS and PbSe Quantum Dots. *J. Opt. Soc. Am. B* **1997**, *14*, 1632–1646.
68. Cragg, G. E.; Efros, A. L. Suppression of Auger Processes in Confined Structures. *Nano Lett.* **2010**, *10*, 313–317.
69. Yu, W. W.; Falkner, J. C.; Shih, B. S.; Colvin, V. L. Preparation and Characterization of Monodisperse PbSe Semiconductor Nanocrystals in a Noncoordinating Solvent. *Chem. Mater.* **2004**, *16*, 3318–3322.
70. de Millo, J. C.; Wittman, R. H.; Fiend, R. H. An Improved Experimental Determination of External Photoluminescence Quantum Efficiency. *Adv. Mater.* **1997**, *9*, 230–238.